Materials and Design 178 (2019) 107860

Contents lists available at ScienceDirect

Materials and Design

journal homepage: www.elsevier.com/locate/matdes

Effect of silsesquioxane addition on the protective performance of fluoropolymer coatings for bronze surfaces

Mohor Mihelčič [a], Miran Gaberšček [a], Martina Salzano de Luna [b,c], Marino Lavorgna [b], Chiara Giuliani [d], Gabriella Di Carlo [d], Angelja K. Surca [a,*]

[a] National Institute of Chemistry, Hajdrihova 19, SI-1000 Ljubljana, Slovenia
[b] Institute for Polymers, Composites and Biomaterials, National Research Council of Italy (IPCB-CNR), P.le E. Fermi 1, 80055 Portici, Italy
[c] Department of Chemical, Materials and Production Engineering, University of Naples Federico II, P.le Tecchio 80, 80125 Naples, Italy
[d] Institute for the Study of Nanostructured Materials, National Research Council (ISMN-CNR), Via Salaria km 29,300, 00015 Monterotondo, RM, Italy

HIGHLIGHTS

- Combination of protective efficiency and removability in anticorrosion coatings suitable for conservation of bronze.
- Homogeneous distribution of POSS nanoparticles in fluoroethylene/vinylether-based coatings.
- Cuprous oxide may form at the bronze|coating interface at high anodic potentials.
- POSS nanoparticles addition enhanced hydrophobicity and protective efficiency while decreasing mechanical properties.

GRAPHICAL ABSTRACT

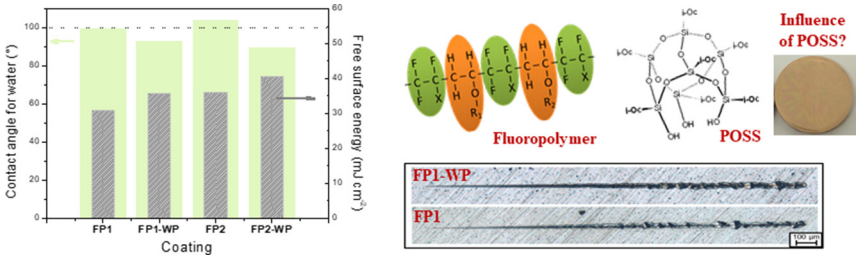

ARTICLE INFO

Article history:
Received 11 March 2019
Received in revised form 29 April 2019
Accepted 14 May 2019
Available online 19 May 2019

Keywords:
Bronze
Protective coating
Nanocomposite
Fluoropolymer
POSS nanoparticle
Nanoindentation

ABSTRACT

Two types of innovative coatings based on fluoroethylene/vinylether alternating copolymers are investigated as protective systems for bronze works-of-art. The influence of a polyhedral oligomeric silsesquioxane (POSS), i.e. open-cube trisilanol-heptaisooctyl-POSS, on the surface, mechanical, optical and electrochemical properties of coatings is examined. It is found that the isooctyl groups in the organic shell of POSS cause an increase in the hydrophobicity of the surface. On the other hand, nanoindentation tests show that the reduced modulus, hardness and plasticity index decrease with the addition of POSS, while abrasion resistance is slightly improved. Haze of coatings increases when POSS nanoparticles are present. More importantly, a beneficial effect of POSS addition on the protective efficiency against corrosion is assessed by exposure of coatings to acidic vapours and electrochemical treatments. In this regard, potentiodynamic polarisation clearly shows that the protective efficiency is systematically larger for coatings comprising POSS. The ex situ IR reflection-absorption spectroelectrochemistry shows that cuprous oxide can eventually form at the coating|bronze interface, which is identified through the spectroelectrochemistry of unprotected bronze.

1. Introduction

In the field of cultural heritage conservation, different attempts have been made to protect bronze surfaces, but they have not succeeded to completely overcome wax and Incralac™ [1] that are still considered

* Corresponding author.
E-mail address: angelja.k.surca@ki.si (A.K. Surca).

https://doi.org/10.1016/j.matdes.2019.107860

very attractive options. Most probably, the main reason originates from the conservation ethics demands that the applied protective coatings should be removable from the bronze surfaces. Anyhow, such removability prerequisite is inherently in contradiction with the need for high protective efficiency, since highly protective coatings are dense and are characterized by excellent adhesion to the underlying substrate. Consequently, different approaches should be used to design the structure of the coatings in order to meet the required removability aspect. In the light of these observations, it is not surprising that the studies of the organic benzotriazole films and its derivatives highly dominated this research field [2], as evident from the literature search disclosed in Fig. S1 in *Supporting information*. Surprisingly, an important number of works on bronze protection deals with the sol-gel protective coatings [3]. Specifically, these coatings are not removable, but attract attention due to their ease of application, good adhesion and excellent protective properties. Consequently, it is supposed that they may find an appropriate application in the outdoor bronze protection.

Studies of other types of materials are much rarer (Fig. S1), but the recent attempts tend to the preparation of removable protective systems. Water-soluble chitosan coatings [4] have been suggested to be a promising candidate for the indoor protection of bronze artworks, as well as coatings prepared on the basis of diamond-like carbon (DLC) [5], and polyvinyl alcohol (PVA)-based coatings containing layered double hydroxide nanocarriers [6]. For the outdoor protection, the bet has been laid on various polymeric materials. Consequently, investigations of polyurethanes [7,8], methyl methacrylates [9], and fluoropolymers [10–12] could be found in the literature. Most of these studies were performed on patina-free bronze surfaces, although patina can form on the bronze surfaces under exposure to air [1], or can even be intentionally induced for protective and coloristic reasons by the artists themselves [13].

In the case of works of art exposed in outdoor environments, fluoropolymers stand out as a potential solution thanks to their weathering resistance. Firstly, coatings based on polyvinylidene difluoride (PVDF) building blocks (-CH_2-CF_2-) were examined on patina-free bronze surfaces [10], but the adhesion was not sufficient. Although PVDF fluoropolymers exhibit an outstanding durability, high temperature treatments are often required for their processing. In addition, the coating adhesion to substrates is generally rather poor and they are quite soft, which reflects their thermoplastic nature. In the last decades, these shortcomings have been successfully overcome thanks to the development of fluoroethylene vinylether (FEVE) fluoropolymers [14,15]. FEVE fluoropolymers have -CF_2-CFX- building blocks and functional groups attached to the polymer backbone (Fig. 1A). Consequently, they can be processed at lower temperatures with respect to PVDF-based fluoropolymers, the resulting coatings are harder and, most importantly, the adhesion to underlying substrates is considerably improved. At the same time, the outstanding durability against weathering remains a peculiar characteristic also for FEVE fluoropolymers.

In this regards, our group has already initiated the investigations of the protective efficiency of solvent- and water-borne FEVE fluoropolymer coatings [12], focusing on the comparison of the mechanical, surface and electrochemical properties of compact/highly adhesive coating with an example of the removable one (either solvent- or water-borne). Particular care was also given to the identification of the preparation routes that can ensure the removability of the developed coatings. As possible approaches were identified the use of polyisocyanate with hydrophilic properties, addition of agents that impart strippability, addition of releasing co-solvents, or the use of molar ratio of isocyanate groups of hardener and hydroxide groups of the fluoropolymer resin below unit [12]. An advantage of a simultaneous addition of three additives was chosen as the first preparation route to the solvent-borne coating, removable by benzyl alcohol-based strippers.

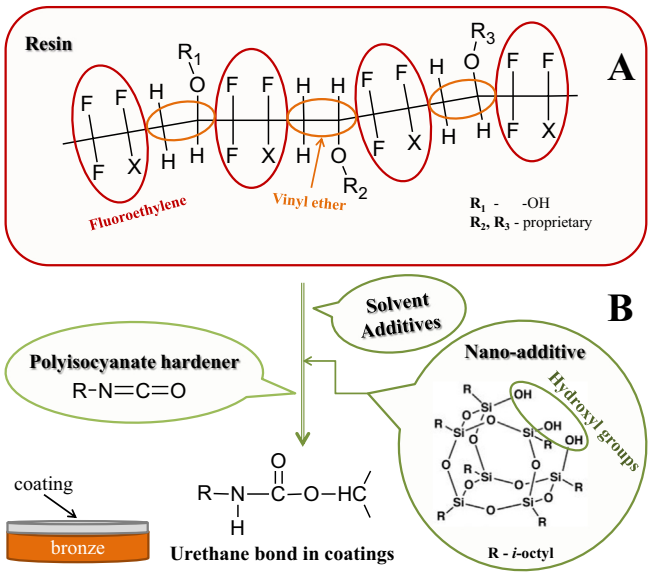

Fig. 1. A) Structure of FEVE fluoropolymer and B) characteristics of the main compounds used in the preparation of FEVE fluoropolymer-based coatings.

An essential property of protective coatings intended for the outdoor application is their water-resistance. In this regard, despite the presence of fluorine groups in fluoropolymers, the hydrophobic character of the coatings can be further increased by the addition of long alkyl groups. As a possible strategy, such groups can be attached to the silica core of polyhedral oligomeric silsesquioxanes (POSS) (Fig. 1B), which are the smallest silica particles in the nature [16]. They are characterized by a general formula $(R\text{-}SiO_{1.5})_n$ ($n = 6, 8, 10, \ldots$), R representing various functionality like hydroxyl, isooctyl etc. The addition of different POSS nanoparticles to polymeric matrices was found to positively influence the scratch, chemical and thermal resistance, as well the electrochemical performance [17]. However, opposing results can also be found in the literature. For example, Lewicki et al. showed that the addition of POSS to polyurethane elastomers did not have any favourable effects [18]. Consequently, we performed an extensive comparison of protective polyurethane coatings for bronze, with and without POSS nanoadditive, which revealed opponent results for different investigated properties [8]. Specifically, the protective efficiency, determined using the electrochemical polarisation, impedance spectroscopy and exposure of coatings to hydrochloric acid vapours confirmed the improved performance of coatings with POSS nanoparticles. Moreover, the contact angle for water, abrasion resistance and ability of the coating in spontaneous recovering after a deformation also increased. In contrast, elastic modulus and hardness were not noticeably affected by POSS addition [8]. Such different responses in properties to the presence of POSS nanoparticles in polyurethane coatings instigated the necessity to examine if the effects caused by POSS addition in the FEVE-based coatings follow any similar pattern.

The main goal of the present work is to prepare new examples of removable solvent-borne FEVE fluoropolymer coatings according to the possible approaches previously identified by our group [12] and to investigate the influence of added trisilanol-heptaisooctyl-POSS nanoparticles on the surface, mechanical, optical and electrochemical performance of the developed coatings. For this purpose, two types of FEVE-based coatings are prepared in a butyl acetate solvent using different additives, as well as two different polyisocyanate hardeners. Energy-dispersive X-ray spectroscopy (EDS) is used to investigate the uniformity of the distribution of trisilanol-heptaisooctyl-POSS nanoparticles in the coatings. The hydrophobicity of the surfaces is determined through static contact angle measurement, while atomic force microscopy (AFM) is applied to calculate the surface roughness. Since

optical fading of protective coatings is unacceptable for art applications, UV-VIS-NIR spectra of coatings deposited on glass are recorded during their exposure to artificial sunlight. Nanoindentation and nanoscratch experiments are expected to reveal the differences in the mechanical properties of the coatings prepared with and without POSS. The protective efficiency of the coatings is tested by electrochemical techniques (potentiodynamic polarisation and impedance spectroscopy (EIS)) and by their exposure to 1 M HCl vapours (accelerated corrosion test). The eventual differences in the accelerated test at the bronze|coating interface are monitored using optical and SEM microscopy. Finally, the eventual changes in the fluoropolymer coatings that occur during forced anodic polarisation are followed with an ex situ infrared reflection-absorption (IR RA) spectroelectrochemical analysis, combining electrochemical treatment and spectroscopic identification.

2. Materials and methods

2.1. Materials preparation

Bronze rods with diameter of 3 cm were obtained from Casa Del Bronzo Srl foundry (Brescia, Italy). As already reported [8], the actual concentration of the main alloying elements in bronze 85,555 was 4.48 wt% of Sn, 5.32 wt% of Zn and 5.24 wt% Pb, 0.10 wt% of Fe and 0.02 wt% of Ni. Polishing of bronze discs was performed first with SiC abrasive paper of P1200 grit, followed by two diamond pastes having particle size of 9 and 3 μm.

The examined protective coatings were prepared on the basis of fluoroethylene/vinylether (FEVE) alternating copolymers (Asahi Glass Company, Japan), as depicted in Fig. 1A. The resin used was Lumiflon LF-200 that was designed for weather resistant coatings and is adapted for solvent-borne formulations. Two different commercially available polyisocyanate hardeners based on hexamethylene diisocyanate (HDI) were used for the preparation of the coatings hereinafter named as FP1 and FP2, respectively: Desmodur N75 (approximately 75% in a 1:1 blend of 1-methoxy-2-propylacetate and xylene) and N3900 (100% resin) received from Covestro supplier (Covestro AG, Germany) (Table 1). The N3900 hardener based on aliphatic HDI, while N75 hardener based on aliphatic HDI biuret, which can supposedly promote the crosslinking and consequently, lead to production of thicker FP1 coatings (Table 1). When on a larger scale, the precursors for the coatings are meant to be delivered as a two-component system (Table 1). Specifically, admixing of Component B (hardener) to Component A should be performed just before the deposition since it induced the crosslinking reaction.

At the laboratory scale, for both types of coatings (FP1 and FP2), in the first step, the LF-200 resin was dissolved in butyl acetate (Table 1; Fig. S2 in *Supporting Information*), and then the nano-additive (Fig. 1B), i.e., trisilanol-heptaisooctyl-POSS (Hybrid Plastics), was added. As light stabilizers Tinuvin 1130 and 292 were used. Tinuvin 1130 is a hydroxyphenyl benzotriazole-based UV absorber, which can be used together with the light stabilizer of the sterically hindered amine class (Tinuvin 292). Additives were included in both coating formulations with the aim of achieving removability of coatings using benzyl alcohol-based strippers, according with the ethical standards for protective coatings for works-of-art. All these compounds compose Component A and they were thoroughly mixed using dispermat dissolver (15 min).

As the second step, polyisocyanate hardener (Component B) was added and the formulations FP1 and FP2 were stirred using dispermat dissolver for 30 min. During this step, the reaction between –OH groups of the resin or POSS with isocyanate groups of the hardener occurred. The pot-life was consequently limited to some hours. After mixing, the coatings were deposited on bronze discs using spin-coating (Fig. S2). First, deposition was performed for 5 s using 500 rounds per minute (RPM) (spin-up), followed by 60 s of spin-off stage with 700 RPM. The deposited coatings were finally thermally treated at 60 °C for 1 h.

In order to get evidence about the influence of trisilanol-heptaisooctyl-POSS nano-additive on protective coatings, formulations without POSS were also prepared (Fig. S2). The resulting coatings were designated as FP1-WP and FP2-WP (WP abbreviation stands for "without POSS").

Removability of coatings was addressed by using a stripper prepared from benzyl alcohol, tetraethylene glycol and Triton X100. Drops of this stripper were deposited on coated bronze disc, left there for 30 min and then removed by using soft cotton tissue.

2.2. Characterisation techniques

Static contact angles were determined for water, formamide and diiodomethane. The measurements were performed on theta tensiometer Biolin Scientific at room temperature. Droplets of liquid (4 μL) were gently deposited on the surface of the coating using a microsyringe. Digital video camera was used to capture the images that were analysed by One Attention Software for contact angle determination. The measurements were repeated three times and average values of contact angles for each liquid were calculated. The free surface energy values were calculated using a set of three Young equations on the basis of contact angles of all three different liquids according to van Oss approach [19]. Necessarily, all three liquids should have known values of total free surface energy (σ_L^{tot}), dispersive part (σ_L^{LW}), electron acceptor (σ_L^-) and electron donor (σ_L^+) components.

Taylor Hobson Series II profilometer was used to measure the thickness of the coatings. The steps for measurements were made by application of a sticky tape on the substrate prior the spin-coating deposition. Sticky tape was removed prior the measurement with the profilometer.

Table 1
Compositions of formulations for preparation of FP protective coatings and the coating thicknesses.

Two-component system	Component	Compound	FP1 (wt%)	FP1-WP (wt%)	Compound	FP2 (wt%)	FP2-WP (wt%)
	Resin	Lumiflon 200	35.0	35.7	Lumiflon 200	20.0	20.4
	Solvent	Butyl acetate	48.8	49.8	Butyl acetate	72.2	73.7
	Nano-additive	POSS	2.0	/	POSS	2.0	/
	Additives	DA	5.0	5.1	TEG	2.0	2.0
		Byk 333	0.2	0.2			
	Light stabilizers	Tinuvin 1130	0.8	0.8	Tinuvin 1130	0.5	0.5
Component A		Tinuvin 292	0.4	0.4	Tinuvin 292	0.2	0.2
Component B	Polyisocyanate hardener	Desmodur N75	7.8	8.0	Desmodur N3900	3.1	3.2
	Coating		FP1 (μm)	FP1-WP (μm)		FP2 (μm)	FP2-WP (μm)
	Thickness		4.2	4.9		1.4	1.2

The coatings were deposited on one side of glass slides for detection of transmittance spectra. The spectra were recorded on a UV-VIS-NIR Perkin Elmer Lambda 950 spectrophotometer in the spectral range from 250 to 2500 nm. The transmittance spectra were first measured for initial coatings. Then, the coatings were exposed in a Suntest chamber (160 W m^{-2}) for 135 and 670 h. The estimation of the optical quality of the coatings was made by determination of a haze value according to an ASTM test method D1003. The definition of the haze is a ratio of diffuse to total transmittance in the range between 380 and 700 nm.

Nanoindentation and nanoscratch experiments were performed with a NanoTest Platform (Micro Materials Ltd) equipped with a standard three-sided pyramidal Berkovich probe. For nanoindentation tests, the penetration depth of the indenter tip was monitored while it was driven to indent the surface of the coating for increasing load values with a loading rate of 0.1 mN s^{-1}. The maximum achievable penetration depth was fixed within 10% of the sample thickness in order to avoid the interference of the underlying metallic substrate [20]. To avoid residual viscoelastic effects, a holding time of 60 s at the maximum load achieved during the loading phase was set before unloading. For statistical purposes, 10 tests were performed for each coating with a 50 μm of distance between adjacent indentations to exclude interaction effects. From each loading-unloading curve, the hardness, H, and reduced elastic modulus, E_R, of the coatings were calculated according to the following relationships, respectively:

$$H = \frac{L_{MAX}}{A_C} \tag{1}$$

$$E_R = \frac{\sqrt{\pi} S_{MAX}}{2\sqrt{A_C}} \tag{2}$$

where L_{MAX} is the indentation maximum load, A_C represents the projected contact areas between the indenter tip and the testing substrate, and S_{MAX} is the slope of the unloading curve at the point of maximum load (i.e. unloading stiffness).

In addition, the relative plastic/elastic character of the investigated coatings can be analysed by referring to the plasticity index, P, which allows to distinguish between recoverable and unrecoverable deformations [21]. It was calculated as:

$$P = \frac{W_P}{W_P + W_E} \tag{3}$$

where W_P is the area encompassed between the loading and unloading curves and corresponds to the plastic work done during indentation, whereas W_E is the area under the unloading curve and represents the viscoelastic recovery.

Nanoscratch tests were performed to assess the scratch and wear resistance of the developed coatings. In each experiment, the coating was solicited at a scan velocity of 1 μm s^{-1} with scratch loads progressively increasing up to 50 mN over a scratch length of 2 mm. Three independent tests were performed for each coating, setting 200 μm of distance between consecutive scans to avoid interaction effects. At the end of the experiments, the tested portion of the materials was inspected by the optical microscopy to investigate the extent of damage produced.

Accelerated corrosion test was assembled for testing of the water-soluble protective coatings for works of art. In this test, the coatings are exposed to vapours of 1 M HCl_{aq} solution at 50 °C, but were not in a direct contact with the acid. Detailed procedure on this test has already been described in Refs. [4–6]. The coated bronze disks were characterized before and after the accelerated corrosion tests. The optical microscopy analysis was carried out using a Leica MEF4M microscope equipped with a digital camera (Leica DFC 280). Morphological images were recorded by means of a SEM Cambridge 360 equipped with an energy dispersive X-ray spectrometer (EDS) INCA 250.

An Autolab PGSTAT 302 N potentiostat-galvanostat equipped with a Frequency Response Analysis system (FRA) module was used for the electrochemical measurements. Potentiodynamic polarisation curves were made in a flat corrosion cell K0235 (Princeton Applied Research). The coated bronze disc was mounted as a working electrode with a geometrical area of 1 cm^2. Polarisation was performed versus an Ag/AgCl/KCl_{sat} reference electrode, while a Pt grid was applied as a counter electrode. The corrosion cell was filled with 0.5 M NaCl electrolyte. Prior to the linear sweep voltammetry from −1.4 to 0.9 V the sample was hold 1800 s at an open circuit potential. The scan rate used for polarisation was 1 mV s^{-1}. The above described corrosion cell was also used for the EIS measurements in the frequency range of 10^5 to 10^{-2} Hz. The perturbation amplitude used was 0.01 V. The samples were exposed to 0.5 M NaCl electrolyte during the period of 6 days.

2.3. Ex situ IR RA spectroelectrochemistry

An insight into the fluoropolymer coatings can be obtained using vibrational Near Grazing Incidence Angle (NGIA) infrared reflection-absorption (IR RA) spectroscopy (Fig. S3 in *Supporting information*). Ex situ IR RA spectroelectrochemical technique combines electrochemical and spectroscopic technique. The coating on bronze is first chronocoulometrically treated at a certain potential in the usual electrochemical cell. After cleaning and drying, the sample is transferred into a specular reflectance accessory in the sample compartment of IR spectrometer (Fig. S3 in *Supporting information)* and the IR RA spectrum recorded. Exposure of the coating to the increasing anodic potential gradually enlarged the load to which the coating was exposed, stimulating the forced degradation. Any piece of information on degradation paths of the coatings (bond cleavage, hydration, …) can offer iterative opportunities for the modification of the coatings with the aim of achieving more stable ones. Ex situ IR RA studies have already been made on sol-gel protective coatings [22,23], but their application has just recently been extended to fluoropolymer [12] and polyurethane [8] coatings.

Ex situ IR RA technique is adapted for thin coatings, being of nanometer thickness range. Since the incidence IR radiation falls at the surface of the coating at a near grazing condition (in our case 80°) and is P-polarised (Fig. S3 B in *Supporting information*), only the bands, the dipole moments of which vibrate perpendicularly to the surface of the coating, appeared in the IR RA spectra. These bands in IR RA spectra correspond to longitudinal optical (LO) modes. These modes are usually shifted with regard to the transversal optical (TO) modes that appear in IR absorbance spectra. The LO-TO splittings are considerable for inorganic coatings, but the shifts are much less notable for organic compounds [24]. More details on ex situ IR RA spectroelectrochemical technique can be found in Ref. [23].

For ex situ IR RA measurements, the Autolab PGSTAT 302 N potentiostat-galvanostat was also used. The rear-side and the edges of the sample, i.e. the coating on the bronze disc, were protected with an epoxy shield on the basis of Epofix resin and hardener (Struers). Then, the sample was exposed as a working electrode to 0.5 M NaCl electrolyte in a usual electrochemical cell. The counter electrode was a Pt rod and the reference electrode Ag/AgCl/KCl_{sat}. The sample was then chronocoulometrically treated at different potentials from −1 to 0.8 V vs. Ag/AgCl/KCl_{sat}. After each chronocoulometric treatment the sample was dismounted from the electrochemical cell, cleaned under a flow of miliQ water and dried in a flow of nitrogen, and finally transferred to the near-grazing IR RA specular reflectance accessory (Fig. S3 A in *Supporting information*) in the sample compartment of the Bruker IFS 66/S spectrometer. Spectroscopic measurement was made using P-polarised light and incidence angle of 80°. The schematic representation of the beam path is depicted in Fig. S3 B. The same coating (either FP1 or FP2) was used for the whole ex situ experiment, i.e. measurements at all potentials.

3. Results and discussion

3.1. Characterisation of coatings

3.1.1. Surface properties of coatings

EDS analysis was employed to investigate how POSS nanoparticles distribute within the coatings. As evident from Fig. 4A,B, silicon is homogeneously distributed in FP1 and FP2 coatings, consequently, trisilanol-heptaisooctyl-POSS nanoparticles. The good distribution of POSS nanoparticles resulted from thorough mixing of Component A (resin, solvent, additives) before the addition of B component, i.e., polyisocyanate hardener (Table 1, Fig. S2). Specifically, the hydroxyl groups of POSS open cubes can - as the hydroxyl groups of the resin - take part in the reaction with the polyisocyanate hardener (Fig. 1). In a well-mixed system, POSS nanoparticles can be successfully and evenly incorporated in the polymeric matrix of the coating (Fig. 2A,B). The SEM images of FP1 and FP2 coatings confirmed the homogeneity of the surface (Fig. 2C,D).

Hydrophobic properties of the coatings usually correlate with their protective efficiency. In Table 2, the contact angles for water are reported in addition to the contact angles of diiodomethane and formamide. Comparison of the pristine fluoropolymer coatings without POSS pointed out slightly smaller contact angle for water in case of FP2-WP coating (89.2°) versus FP1-WP coating (92.8°). Bronze disc had a higher contact angle for water of 104.6° [8]. Hardeners (Desmodur N75 or N3900) in both types of coatings consist of aliphatic polyisocyanate of HDI type, but tetraethylene glycol in FP2-WP coating could influence an increase in an electron-donor parameter σ^- and consequently, the polar σ^{AB} component (Table 2). As expected, the addition of the trisilanol-heptaisooctyl-POSS triggered an increase in the hydrophobicity of both types of coatings. Namely, the contact angle for water of FP2 coating increased to 103.8°, while it reached 99.4° for FP1 coating. Such a result evidences that the presence of long alkyl chains in the structure of trisilanol-heptaisooctyl-POSS increased the coating hydrophobicity, as already reported for other systems. An example is sol-gel protective coating prepared on the basis of cyclotetrasiloxane, the hydrophobicity of which significantly increased after the addition of hexadecyltrimethoxysilane [22].

The free surface energy values were calculated from the contact angels obtained for water, diiodomethane and formamide (Table 2). The lowest value was found for FP1 (30.9 mJ m^{-2}), followed by FP1-WP and FP2 coatings, reaching values around ~35 mJ m^{-2}. The highest free energy value was observed for FP2-WP (40.6 mJ m^{-2}), which was also characterized by the lowest contact angle for water. The calculated values σ^{tot} showed that the presence of trisilanol-heptaisooctyl-POSS in the structure of both types of the fluoropolymer coatings led to a decrease of the free surface energy value of approximately ~5 mJ m^{-2}. Such results show that the wettability of the coatings containing POSS by water is lower compared to the pristine coatings prepared without POSS.

Table 2
Static contact angles, free surface energy values and surface roughness of FP1 and FP2 with and without POSS (FP1-WP, FP2-WP).

Coating	Θ_{H2O}	Θ_{CH2I2}	Θ_{NH2CHO}	σ^+	σ^-	σ^{LW}	σ^{AB}	σ^{tot}	SR
FP1	99.4	56.7	78.2	0.04	1.3	30.5	0.5	30.9	231
FP1-WP	92.8	50.0	74.3	0.2	3.4	34.3	1.5	35.8	732
FP2	103.8	57.6	93.0	2.4	3.9	29.9	6.0	35.9	194
FP2-WP	89.2	48.1	77.3	0.9	7.6	35.3	5.2	40.6	621

Θ - contact angles for water, diiodomethane and formamide in °. SR – Surface roughness in nm.
σ^+ – electron donor component; σ^- - electron acceptor component; σ^{LW} – dispersive part;
σ^{AB} – polar part; σ^{tot} – total surface energy value. σ^+, σ^-, σ^{LW}, σ^{AB}, σ^{tot} in mJ m^{-2}.

A comparison of AFM images of coatings with and without POSS clearly reveals the presence of POSS nanoparticles on the surface (Fig. S4 in *Supporting information*). Specifically, the nanostructured features blur the AFM images of FP1 and FP2 coatings with POSS (Fig. S4 A, C) when compared to coatings without POSS (Fig. S4 B,D). This evidence is in line with the above described differences in contact angles for water and free surface energy values. Interestingly, AFM images of FP1 and FP2 series reveal different characteristics reflecting two types of polyisocyanate hardeners used for their preparation. The images of FP1 and FP1-WP coatings showed ridged surface with circular surface lowerings of 0.3 to 1 μm in diameter. This is a consequence of the application of aliphatic HDI biuret hardener that tends to higher crosslinking due to its branched structure. On the other hand, the topography changes are more gradual for FP2 and FP2-WP coatings (aliphatic HDI hardener), but also reach large differences in height. Overall, the surface roughness of 194 nm measured for FP2 coating is slightly lower than the value of 231 nm found for FP1 coating (Table 2). The surface roughness was considerably larger for coatings without POSS, being 621 nm for FP2-WP and 732 nm for FP1-WP (Table 2).

3.1.2. Mechanical properties of coatings

Since POSS nanoparticles were found to increase the hydrophobicity of the prepared fluoropolymer protective coatings, the next step of the study was directed towards the assessment of the effect of POSS addition on the mechanical properties of the coatings. Nanoindentation and nanoscratch experiments were exploited for this purpose. Representative loading-unloading nanoindentation curves for the two types of the investigated coatings are shown in Fig. 3. The most evident information is that the addition of POSS nanoparticles reduces the resistance to the applied load of the coatings, since lower loads are required to induce the same indenter penetration for both the investigated systems. It

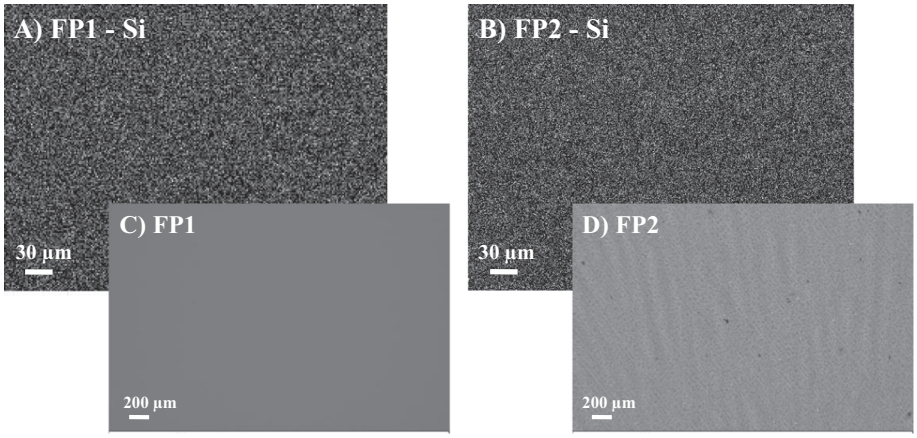

Fig. 2. Distribution of silicon recorded by EDS in fluoropolymer coatings: A) FP1 and B) FP2. SEM images are also depicted: C) FP1 and D) FP2.

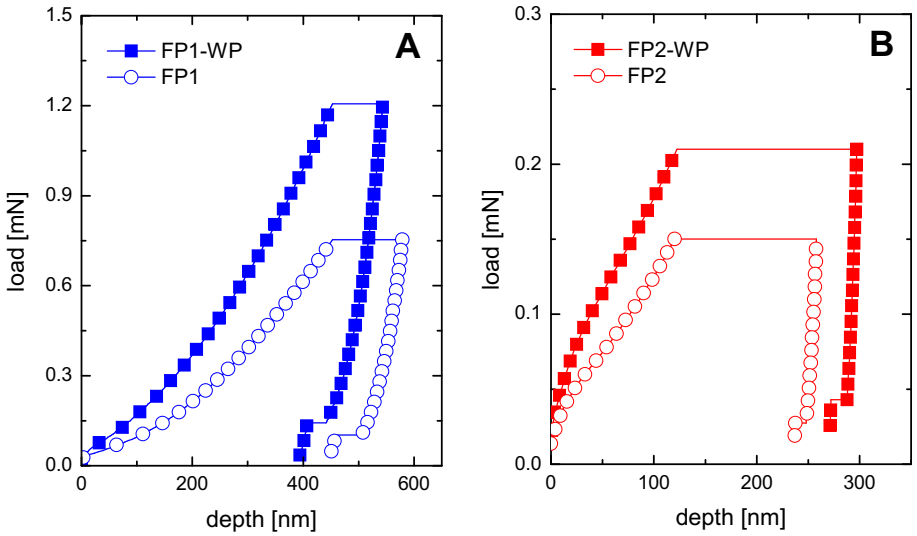

Fig. 3. Representative loading-unloading curves of coatings from nanoindentation tests: A) FP1 and FP1-WP, and B) FP2 and FP2-WP.

should be noted that the maximum achieved depth is different for the two types of systems (FP1 and FP2 series) because of the different coating thickness (Table 1). Indeed, for a reliable comparison of the mechanical properties, the maximum penetration depth was set not to exceed one tenth of the coating thickness (see experimental section). A comparison of the mechanical performances of the developed coatings can be instead obtained by looking at the calculated values of reduced elastic modulus, hardness and plasticity index, which are all reported in Fig. 4.

The reduced elastic modulus of the pristine coatings (FP2-WP and FP1-WP) is essentially the same (5.5–5.8 GPa). On the other hand, the FP1-WP coating is characterized by a much higher hardness value (>4 times) than found for FP2-WP. Thus, the selection of Desmodur 75 polyisocyanate as crosslinker provides a beneficial effect from the viewpoint of the mechanical performances. The HDI biuret-based structure of this hardener promote the tendency to crosslinking, as it may assure more covalent and secondary crosslinking bonds. For the FP2 and FP1 series of samples, the addition of POSS nanoparticles has a detrimental effect on both E_R and H (Fig. 4A,B). Similarly, Ghermezcheshme et al. [25] also reported a decrease of elastic modulus and hardness of polyurethane coatings upon addition of different kinds of POSS nanoparticles. There are two possible reasons for this effect. Firstly, POSS nanoparticles may induce an increase of the free volume of the systems due to interactions among POSS open-cages and polymer chain segments [26] and/or can crosslink with the -NCO groups of polyisocyanate. Differential scanning calorimetry (DSC) analyses performed on the developed materials revealed that the addition of POSS nanoparticles lowered the glass transition temperature of the polymer matrices for both the FP1 and FP2 formulations (Fig. S5). This result suggests that the detrimental effect of the POSS nanoparticles on the mechanical performances of the coatings can be related to an increase of the free volume of the polymeric matrices.

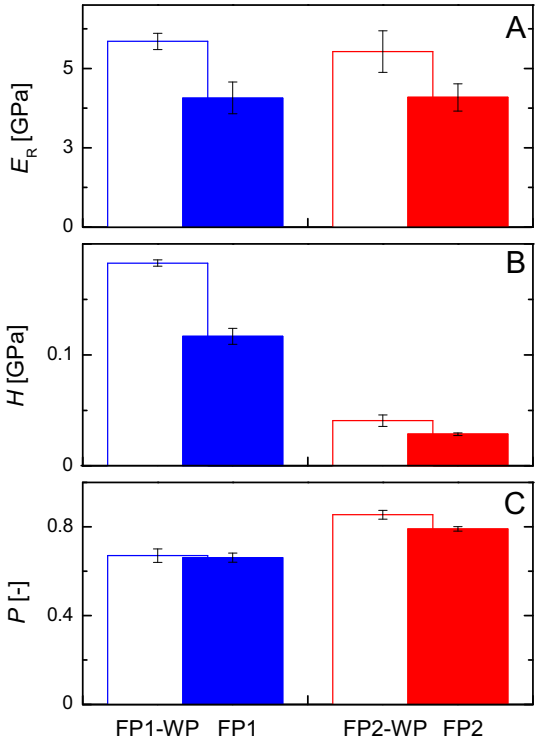

Fig. 4. A) Reduced modulus, B) hardness and C) plasticity index for the FP1 and FP2 coatings with and without POSS addition.

Alternatively, the analysis of the plasticity index reveals that it is only slightly influenced by the addition of POSS nanoparticles. It is worth noting that the value of P for the FP1 series is lower than that for the FP2 one (Fig. 4C), indicating that the FP1-WP and FP1 coatings are characterized by a higher elastic connotation, which is expected to improve the ability of spontaneously recovering after the deformations, eventually conferring a better wear resistance to the coating. Actually, a similar conclusion can be also drawn by looking at the H/E_R ratio, which can be indicative of the wear resistance of coatings [27]. In particular, for high H/E_R values, a good wear resistance is expected. The FP2-WP and FP2 coatings are characterized by lower H/E_R values (~$7 \cdot 10^{-3}$) than FP1-WP and FP1 ones (~$3 \cdot 10^{-2}$). In addition, the H/E_R values for the FP1 series of samples is also slightly higher than those reported by Koumoulos et al. [28] for Teflon-based coatings, suggesting that the developed coatings are promising protective systems in terms of wear resistance. These considerations have been supported and verified through nanoscratch experiments, whose typical output is shown in Fig. 5, in which the representative optical micrographs of the scratch paths and the initial part of the nanoscratch profile curves are reported.

Evidently, the FP2-WP and FP2 coatings are irreversibly damaged even for the very low applied loads. A remarkable pile-up deformation mechanism is observed, the effect being more pronounced for the FP2-WP system (Fig. 5B). This evidence is also confirmed by the profile of the scratch curve, in which the deeper indentations can be noticed for the FP2-WP coating (Fig. 5D), indicating that POSS addition partially improve the abrasion resistance of the FP2 series. On the contrary, the FP1

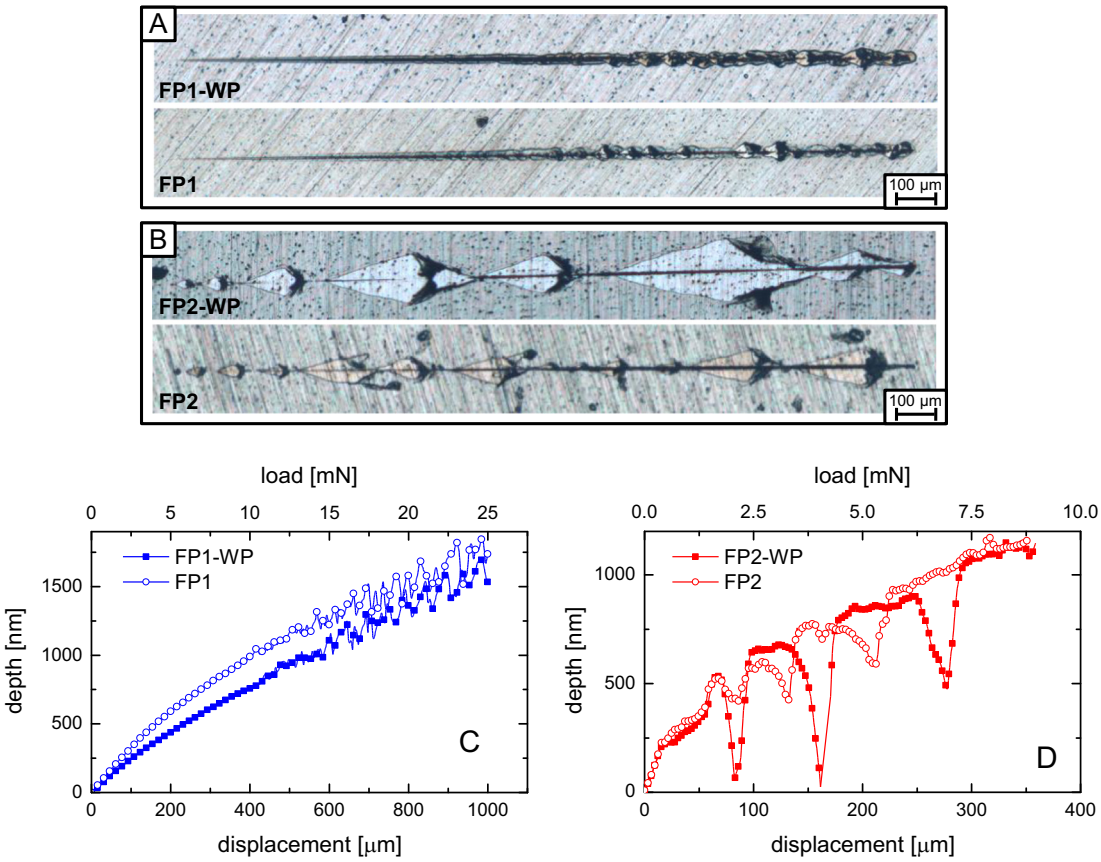

Fig. 5. Representative optical micrographs of the scratch paths on coatings: A) FP1-WP and FP1, B) FP2-WP and FP2. Representative initial part of the nanoscratch curves showing the penetration depth of the indenter as a function of the displacement (bottom x-axis) and the applied load (top x-axis): C) FP1-WP and FP1, B) FP2-WP and FP2.

set of samples is characterized by a remarkably higher wear resistance, as testified by the modest plastic deformation caused during the nanoscratch experiments (Fig. 5A). In this case, the addition of POSS nanoparticles does not have a significant effect. From the nanoscratch curves in Fig. 5C it can be only noticed that the penetration depth is slightly higher for the FP1 system, likely because of the lower hardness with respect to the FP1-WP coating. Nonetheless, the critical load, L_C, that is the load value at which the primary optically observable fracture phenomenon occurs [29], is similar for the two FP1 samples and it is equal to ~14 mN. This is much higher than that found for the FP2 set of samples ($L_C < 1.5$ mN). The different thickness of the two sets of samples prevents from a direct quantitative comparison of the adhesion strength at the coating/substrate interface. Nonetheless, the huge difference in the L_C values is in line with the expectation based on the Tresca's yield criterion and Tabor's relation, according to which the load necessary to initiate a plastic deformation is proportional to the H^3/E^2 ratio that thus indicate the quality of the adhesion between the coating and the substrate [28,30]. The values of H^3/E^2 computed from the data of the nanoindentation tests reported in Fig. 4 are ~10^{-5} and ~10^{-6} GPa for the FP1 and FP2 series of samples, respectively. This difference of about one order of magnitude is in good agreement with the L_C values obtained by the nanoscratch experiments.

3.1.3. Optical properties of the coatings

The transparency of any protective coatings with time of exposure to sun is of large concern for works-of-art. Consequently, in order to determine the optical properties (i.e. transmittance and haze), the fluoropolymer coatings were deposited on glass slides. The transmittance of all initial coatings approaches 90%, with a steep decrease below 400 nm (Fig. 6A,B). The investigated coatings were then exposed to artificial sunlight. At wavelengths above 800 nm the exposure for 135 and 670 h did not induce any change in transparency. Some changes were, instead, noted in the range 400–800 nm, being much less evident for FP2 series than for FP1 one. Anyhow, the interesting point is that for both series of samples, the larger decrease in transmittance was noted for coatings with POSS than for coatings without POSS.

Consequently the haze, i.e., the parameter that mainly refers to the quality of the coatings, especially if coatings contain nanoparticles, was determined. Haze was lower for the coatings without trisilanol-heptaisooctyl-POSS than for the coatings with POSS and it was below or equal to 0.5 for most of the developed coatings (FP2, FP2-WP, FP1-WP) (Fig. 6C,D). For these coatings, exposure in a Suntest chamber led to slight increase in haze values, up to 1.9. In contrast, the initial haze value of FP2 coating was 6.4, which further increased to 7.0 after 670 h of exposure. This large value of haze confirmed the change in transmittance during the exposure in the wavelength range of 400–800 nm (Fig. 6A).

3.2. Protective efficiency of the coatings

3.2.1. Accelerated corrosion test

In order to assess the protective efficiency of the developed coatings, the accelerated corrosion tests were carried out. In particular, the coated bronze substrates were exposed to 1 M HCl acidic water vapours to accelerate the corrosion processes and to rapidly get information about their protective efficiency. To evaluate the ability of the coatings to inhibit the degradation of the underlying alloy substrate, the coated disks were characterized before and after the accelerated corrosion tests by optical microscopy (Fig. 7).

After 12 h of the accelerated corrosion treatment, FP1 coatings with and without POSS are still stable, transparent and there is no evidence of the formation of corrosion products at the metal|coating interface. As

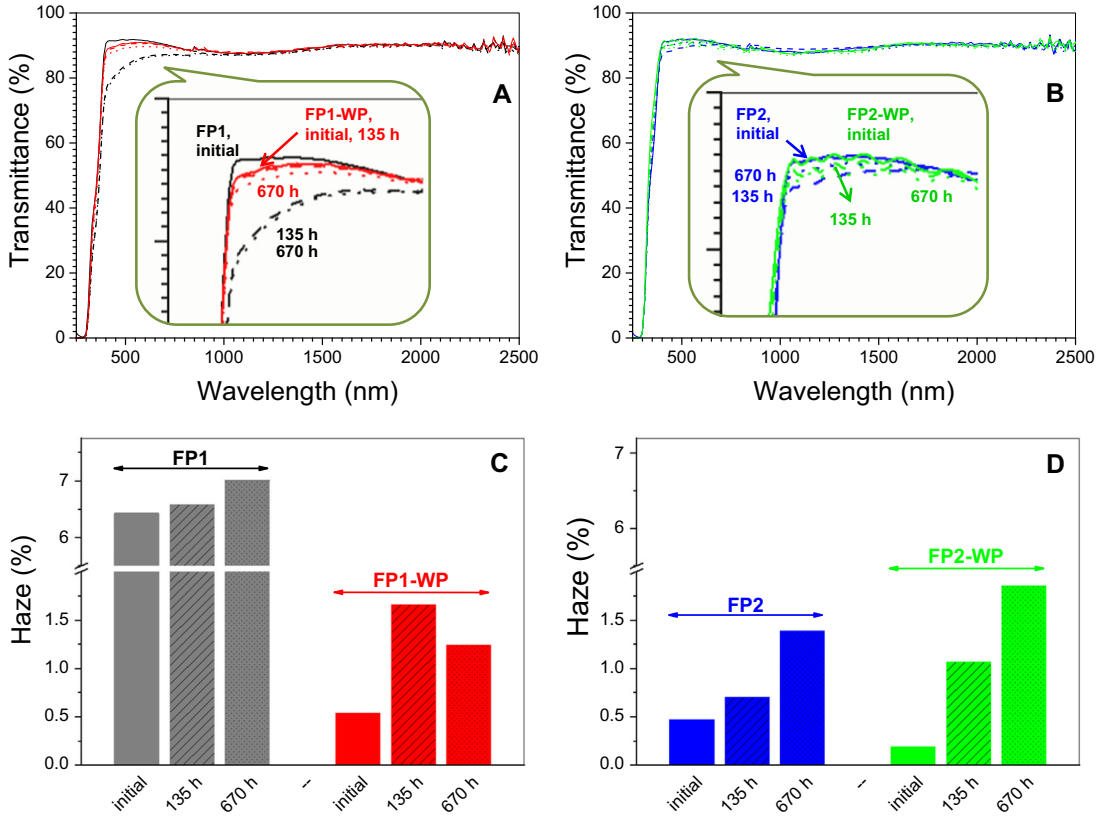

Fig. 6. A,B) Transmittance spectra and C,D) haze of the coatings in the initial state and after the exposure in Suntest for 135 and 670 h: A,C) FP1 and FP1-WP, B,D) FP2 and FP2-WP.

clearly shown by optical micrographs in Fig. 7C,D, the alloy substrates remain unchanged after the corrosion treatment, thus demonstrating the efficiency of these coatings in inhibiting the corrosion processes. On the contrary, in the case of both FP2 formulations, the exposure to aggressive vapours led to the loss of the coatings' transparency and to a modification of the bronze substrate appearance.

SEM analysis confirmed the difference between the FP1 and FP2 series of coatings after the accelerated corrosion treatments (Fig. 8). Specifically, SEM images of coatings after treatment showed large aggregates within FP2 and FP2-WP coatings, whereas no aggregates were detected in the FP1 and FP1-WP analogues. While no significant beneficial effect of POSS addition was observed for FP1 vs. FP1-WP coatings, the presence of POSS had some beneficial effects on its protective properties in the FP2 coating. Namely, the modification of the alloy substrate after 12 h of corrosion test was more pronounced for FP2-WP with respect to FP2. Further investigations by EDS analysis revealed that the aggregates in FP2 consisted of different ratios of Cl, Cu, Pb, O, F and Si suggesting the formation of the degradation products (Fig. 9). Silicon and fluorine originated from the disintegrated coating, Cl deposited from the chloride-containing acid vapours, while Cu and Pb came from 85,555 bronze discs. Pb is the only alloying element in 85,555 that is not bounded in any phase [31,32].

3.2.2. Electrochemical characterisation of the coatings

Potentiodynamic polarisation measurements (Fig. 10) confirmed the findings of the accelerated corrosion tests (Fig. 7). The protective efficiency of the coatings, indeed, was somewhat improved by the addition of trisilanol-heptaisooctyl-POSS. Specifically, the decrease in the anodic current density of FP1 coatings with regard to uncovered bronze disc was of about five orders of magnitude. In contrast, that decrease

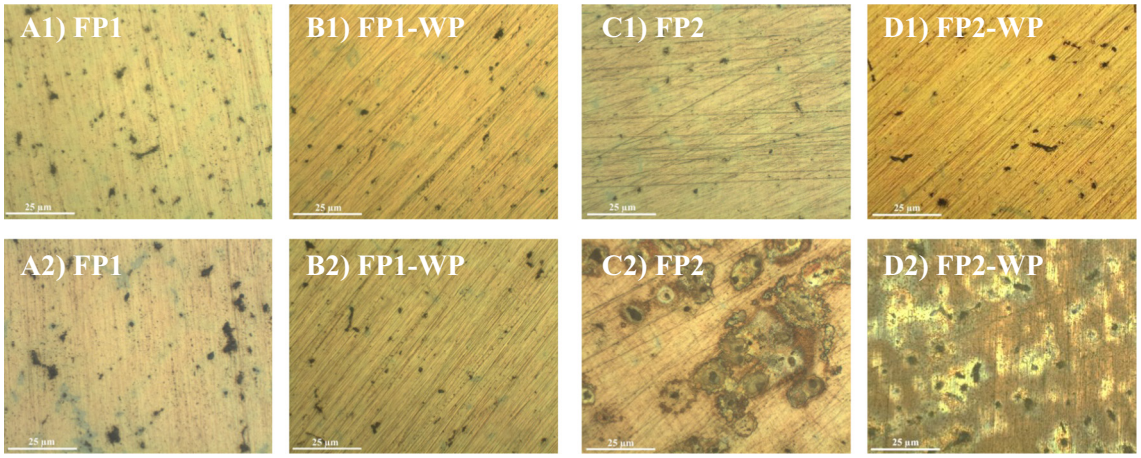

Fig. 7. Optical images of the bronze discs covered by FP1 (A), FP1-WP (B), FP2 (C) and FP2-WP (D) protective coatings before (1) and after (2) the accelerated corrosion treatment for 12 h.

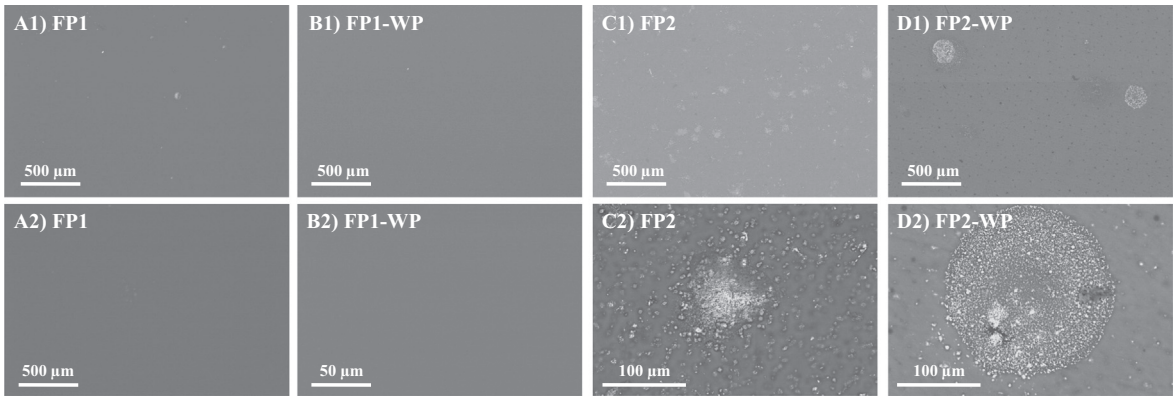

Fig. 8. SEM images of the bronze discs covered by the protective coatings: A) FP1, B) FP1-WP, C) FP2 and D) FP2-WP. SEM images were recorded after the accelerated corrosion treatment (12*h*) using different magnifications (1,2).

was slightly smaller for FP1-WP coating without POSS. A similar situation was noted for FP2 and FP2-WP coatings. A larger decrease in the anodic current density, i.e., better protection efficiency, was noted for FP2 compared to FP2-WP samples. The protection efficiency of the FP1 series was better compared to the FP2-based counterparts, which could be partly linked to the larger thickness of FP1 and FP1-WP coatings, as well to the larger tendency of HDI biuret-based hardener Desmodur N75 for crosslinking (Table 1).

In order to get additional insights into the behaviour of all four kinds of coatings, EIS measurements were carried out. In particular, the goal was to get more information about the stability of coatings as a function of time.

The presentation of Bode plots for the four coatings is shown in Fig. 11 with the same scale for impedance magnitude (Y-axis). In this representation, the corrosion protection ability is roughly proportional to the absolute value of impedance (impedance modulus) at the lowest frequencies. In all coatings, the magnitude of EIS spectra decreases with immersion time (from 0 h to 6 days). Typically, these changes are within one to two orders of magnitude. After a couple of days, the values of low-frequency impedances stabilize in all coatings studied. There are however quite big differences observed when comparing different coating types, i.e., FP1 vs. FP2 samples.

Due to significant scatter of measured impedance values as a function of frequency (see for example the 0 h and 3 h spectra in Fig. 11), it was not possible to analyse reliably the spectra using an appropriate model as proposed in the literature [33]. For this reason, we simply report the low-frequency (0.01 Hz) modulus as a function of time (Fig. 12). Note that the measured modulus of each coating was normalized with respect to its surface area and thickness, in order to obtain a "specific impedance modulus" (by analogy to resistivity, i.e. "specific electrical resistance"), which effectively eliminated the geometrical effects from the comparison.

All samples show a significant drop of moduli ("resistances") during the first couple of hours of immersion. After about 20 h, however, the moduli stabilized. Consistently with the potentiodynamic polarisation experiments, both FP1 coatings exhibit |*Z*| values that are significantly higher (about two orders of magnitudes) than those of FP2 coatings. Note that, in contrast to the potentiodynamic measurements, the impedance values were normalized per thickness and surface area of coatings. In other words, if there is an effect of coating thickness on electrochemistry, it is probably only marginal in the present samples. Furthermore, the relatively rapid variation of impedance during the first couple of hours could at least partly explain the oscillations visible in some of the polarisation curves (Fig. 10). At least during the first day of immersion, the samples without POSS show somewhat lower average impedance moduli which may be correlated to a lower protection ability (Fig. 12).

3.2.3. Ex situ IR RA spectroelectrochemical measurements

Combined electrochemical and spectroscopic ex situ IR RA measurements were performed for FP1 and FP2 protective coatings (Fig. 13). The whole sets of recorded IR RA spectra are depicted in Figs. 13A,B. The bands at 2864 and 2941 belong to symmetric and antisymmetric C—H stretching modes, the bending of which appeared between 1470 and 1440 cm^{-1} [12,34]. In the spectral region 1800–1600 cm^{-1} the characteristic bands of urethane (-NH-CO-O-) groups appeared, which formed during crosslinking of –OH content of resin and isocyanate -NCO groups of the hardener [12,34]. The band at 1130 cm^{-1} reflected the presence of CF_2 and C—O groups from the resin. It is evident that the intensity of the bands decreased with increase in potential, while the positions of the bands remained the same. The intensity decrease is much more evident for FP2 than for FP1 coatings. This can also be the consequence of the thickness difference enabling the molecules of water and other species from the electrolyte a quicker access to the bronze|FP2 coating

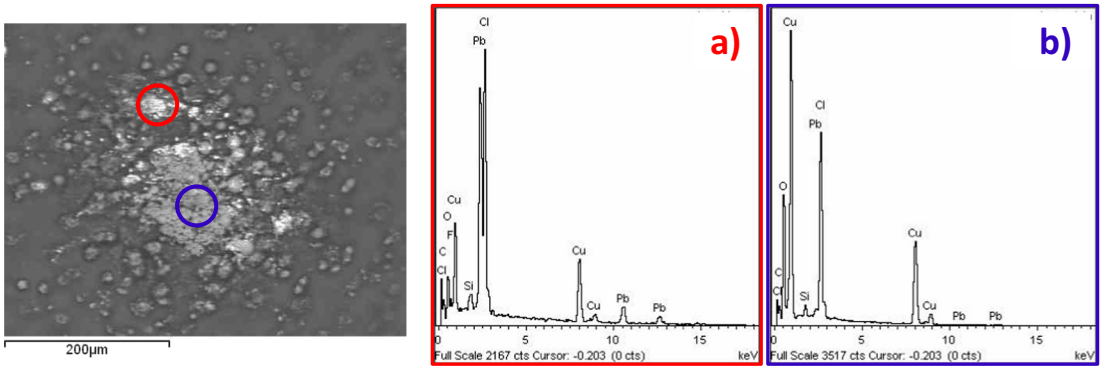

Fig. 9. SEM image and EDS analysis of the aggregates (A,B) that formed in FP2 coating during the accelerated corrosion test (12 h).

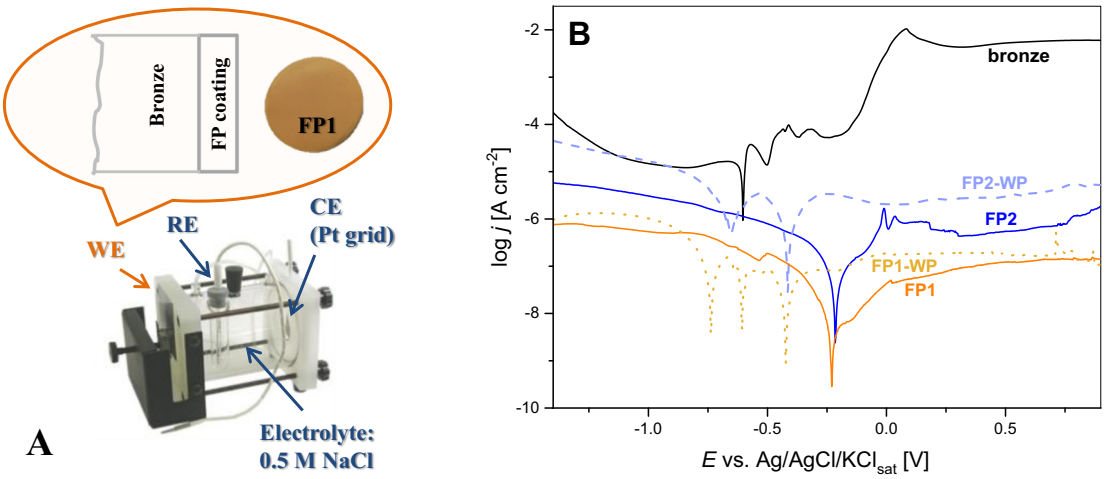

Fig. 10. A) An experimental setup and B) the potentiodynamic polarisation measurements of FP1 and FP2 coatings with and without POSS.

interface. The shape of IR RA spectra of FP2 coatings recorded before and after the corrosion potential (i.e. -0.2 V in Fig. 10) somewhat differ (Fig. 13B). This indicates that the corrosion processes started to influence the interface. Such difference cannot be noticed for FP1 coating (Fig. 13A). These spectra only revealed a moderate decrease in the intensity of bands, which can arise from the manipulation of the coated bronze discs outside the electrochemical cell. In fact, it is much more informative to follow the differences in ex situ spectra during the forced polarisation (Fig. 13B) than to deal with coatings that only show the intensity decrease in all bands (Fig. 13A). Specifically, the IR RA spectra sample along the beam path on the surface of the coating (Fig. S3 B in *Supporting information*), which gives the average result for all processes that occur. Since in good protective coatings the corrosion processes proceed very slowly and only at certain sites, for example, the number of bonds that break in the coating is often too small to be noted in the spectra. Also eventual pitting of coatings can often reflect only in the decrease in the band intensity.

With the aim of getting a deeper insight into the eventual differences in the IR RA spectra, the spectra of the initial and the most anodically polarised (i.e. 0.8 V, 720 s) coatings are directly compared in Figs. 13C, D. According to the differences in the intensities of the bands and the slopes of the spectra, background correction was performed. In addition,

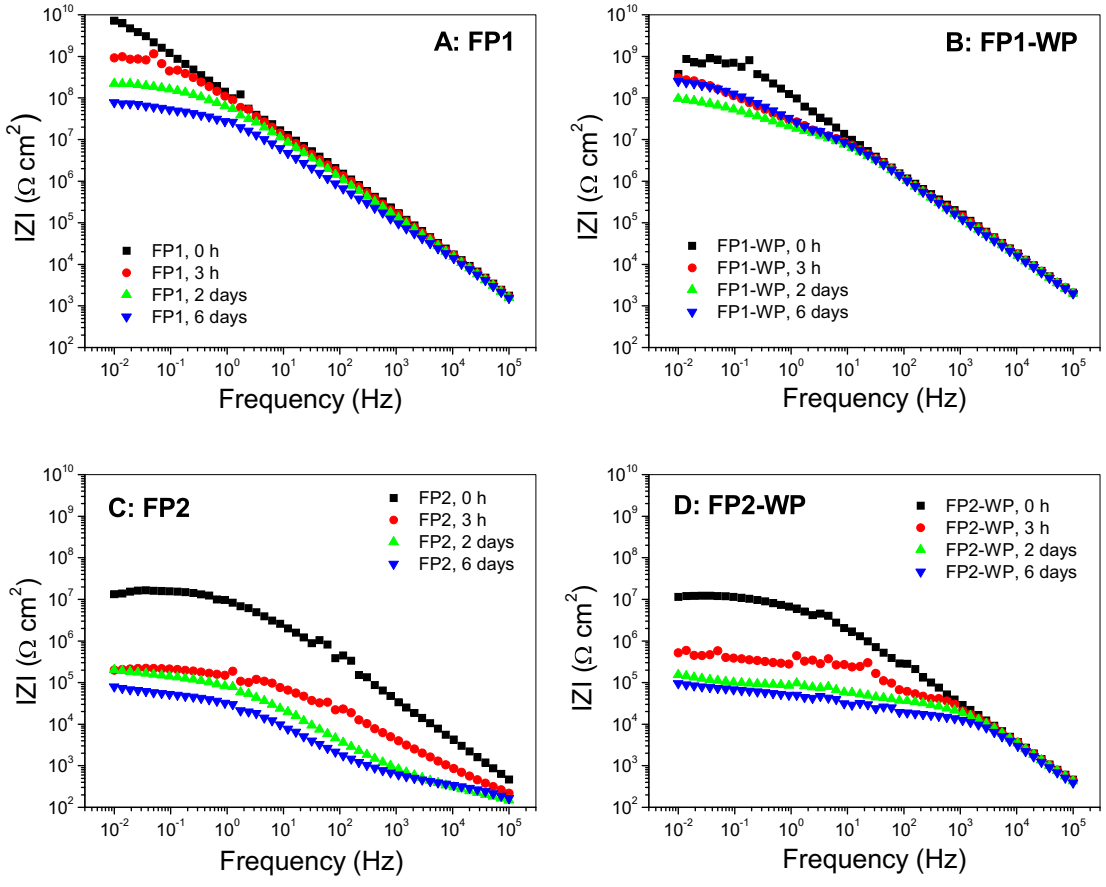

Fig. 11. Bode plots of protective coatings: A) FP1, B) FP1-WP, C) FP2 and D) FP2-WP.

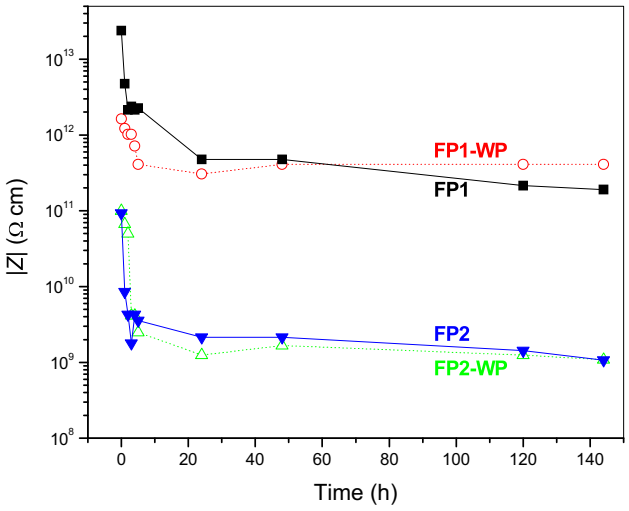

Fig. 12. Time evolution of the low-frequency modulus, |*Z*| (0.01 Hz), for different coatings used in this work.

the spectra were upscaled to C—H modes between 3000 and 2830 cm^{-1}. After correction and upscaling, a broad and quite intense band below 1000 cm^{-1} became visible for FP2 coating (Fig. 13D). Its formation was not surprising according to the differences in the shape of the ex situ IR RA spectra of the FP2 coating recorded before and after the corrosion potential (Fig. 13B). The left band peak that appeared at 765 cm^{-1} has already been present in the initial spectrum of the FP2 coating (Fig. 13B,D). The band centred at 644 cm^{-1}, however, suggested the formation of cuprous Cu_2O oxide at the interface of bronze|FP2 coating. Such feature has already been detected in the ex situ IR RA measurements of water-borne fluoropolymer coating at 656 cm^{-1} [12]. The value of 644 cm^{-1} is close to 617 cm^{-1} [35], 619–627 cm^{-1} [36], 640 cm^{-1} [37] and 645 cm^{-1} [38] bands that were identified in the IR RA spectra as LO modes of Cu_2O. With the aim of verifying this statement, ex situ IR RA spectroelectrochemical measurements were also performed on the uncoated bronze substrate (Fig. 14). It is evident that the exposure of bronze to increasing potential led to formation of a band at 623 cm^{-1} that could be related to the formation of cuprous oxide [12,35–38]. However, at more positive anodic potentials large interference effects became visible in the spectra, which consequently did not support further conclusions.

4. Discussion on influence of POSS on coatings

Addition of various POSS cubes has often been reported [17,39–41] to beneficially influence either scratch, thermal, chemical or electrochemical properties of composite polymeric systems. Such studies are mostly oriented in a direction of a single property, that is why a prospect on behaviour of a POSS-comprising materials is not given integrally. With the aim to verifying the influence of POSS on our developed protective coatings, we prepared coatings with and without trisilanolheptaisooctyl-POSS nanoparticles (Fig. 1B). On these samples, surface, mechanical, optical and electrochemical properties, as well protective efficiency according to the exposure to acidic vapours, were tested. Importantly, the ability of this open-cube POSS to bind into the fluoropolymer system via three silanol groups, prevented the eventual leaching of POSS molecules from the coatings.

As already noted for other systems [39], the functionality of the organic shell of POSS can have large influence on surface properties. Many coatings with incorporated POSS with long alkyl groups or

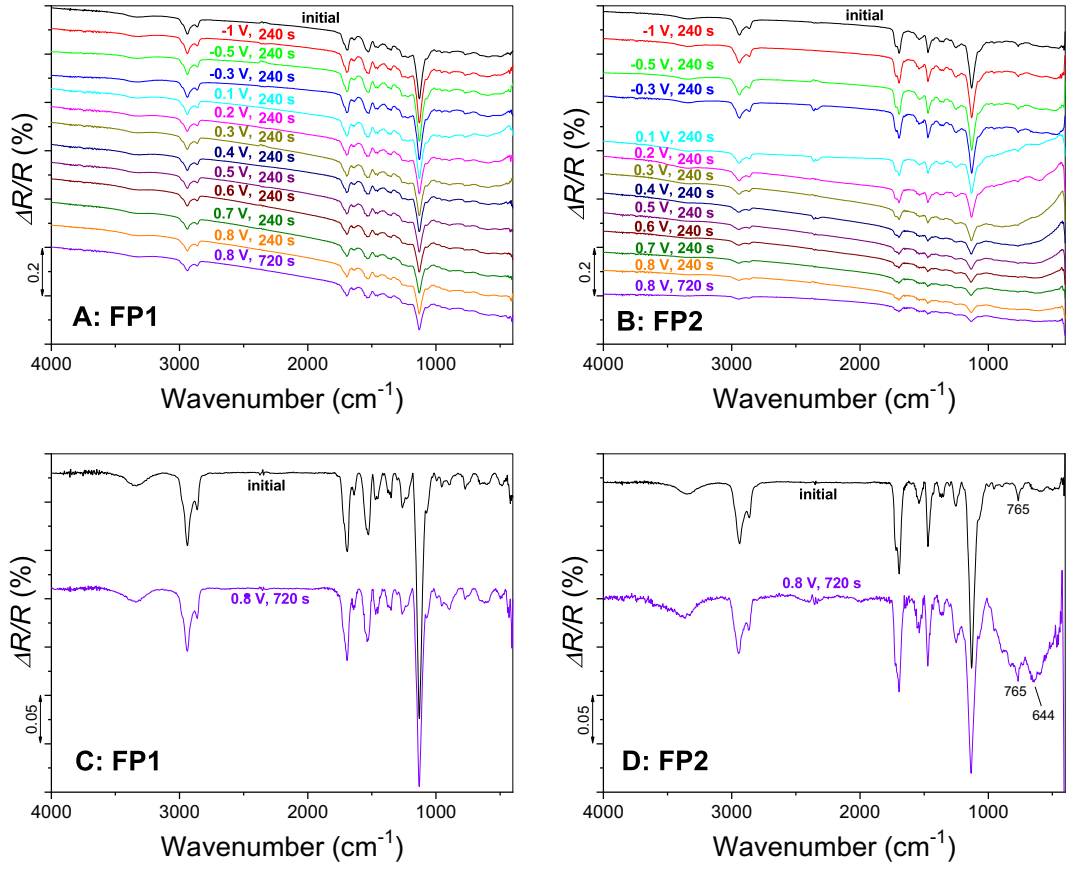

Fig. 13. Series of spectra obtained during ex situ IR RA measurements of coatings on bronze discs: A) FP1 and B) FP2. The initial and the most anodically polarised ex situ IR RA spectra are compared for: C) FP1 and D) FP2 coating.

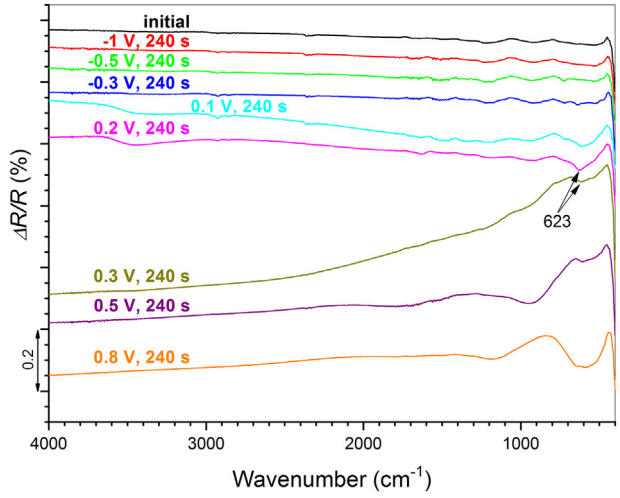

Fig. 14. Series of spectra obtained during ex situ IR RA measurements of a bronze disc.

perfluoro groups were characterized with an immediate increase in the contact angles for water, i.e., increased hydrophobicity, and a decrease in the free surface energy. Due to the improved barrier effect and therefrom ensuing more difficult access of water molecules and other species from the electrolyte to the alloy|coating interface, the beginning of the corrosion processes at the interface is postponed. The same finding was noted also in the case of FP1, FP2 coatings (Table 2) comprising POSS nanoparticles with seven isooctyl groups linked to the seven corners of each molecule.

Nanoindentation experiment showed that FP1, FP2 coatings with POSS have a reduced resistance to the applied load (Fig. 3). As a result, these coatings had a lower reduced modulus, hardness and plasticity index compared to the pristine coatings without POSS (FP1-WP, FP2-WP) additive (Fig. 4). The extent of the decreases was different for the measured parameters, and depended on the type of the coating. Namely, the thickness considerations resulted in the necessity for the adjustment of the measurement depth (10% of the coating thickness). In contrast, nanoscratch experiments revealed that the addition of POSS diminished the pile-up of the matter for FP2 coatings (Fig. 5). This effect was much less evident for FP1 counterparts that exhibited about 4-times larger hardness compared to FP2 types of coatings. The use of polyisocyanate hardener with HDI biuret-based structure (Desmodur N75) can be responsible for the more extensive crosslinking in FP1 and consequently, the larger hardness. However, with the addition of POSS, abrasion resistance was improved for FP2 coatings, while it remained equal in case of FP1 samples. It is obvious that mechanical properties do not alter in the same direction. While abrasion resistance can be improved with POSS addition, reduced modulus, hardness and plasticity index are diminished.

Accelerated corrosion test (Fig. 7-9) and electrochemical techniques (Figs. 10-12) confirmed a better protective efficiency of the coatings with incorporated POSS. The exposure of the coatings during the accelerated corrosion test showed an improvement for FP2 coating with regard to FP2-WP one. Actually, for the latter coating without POSS EDS analysis identified the presence of Cl, Cu, Pb, O, F and Si in the degradation products (Fig. 9). Potentiodynamic polarisation (Fig. 10) revealed the improved protective efficiency with the presence of POSS. The same is confirmed also for initial impedance measurements. However, during 6 days of immersion, these differences ceased out. When the low frequency modulus (normalized with respect to the surface area and thickness) are plotted against time the largest degradation of all coatings during the first day of immersion is confirmed, as well the better protection of coatings with POSS with regard to the coatings without it (Fig. 12).

The ex situ IR RA spectroelectrochemical measurements (Fig. 13) showed that the evolution of cuprous Cu_2O oxide at the interface of bronze|FP2 coating occurred during the gradual chronocoulometric polarisation towards the anodic potentials. The presence of cuprous oxide is confirmed through the formation of broad band at 644 cm^{-1} (Fig. 13D). No such band can be noted for FP1 coating (Fig. 13C). Formation of similar band on the surface of bronze exposed to the same type of ex situ IR RA measurements confirmed the oxidation to cuprous oxide (Fig. 14). It should be stressed that one major criterion for the study of FP1 and FP2 coatings was their removability with benzyl alcohol-based stripper. Such removability was achieved through additives. However, long term removability is the aspect that should be addressed in future.

5. Conclusions

The present work addressed the influence of the addition of trisilanol-heptaisooctyl-POSS nanoparticles to coatings based on fluoroethylene/vinylether alternating copolymers. It was found that the addition of POSS increased their hydrophobicity, and consequently, the protective efficiency was also improved, as shown by electrochemical techniques and the exposure to acid vapours. Rather surprisingly, the mechanical properties did not follow the improved protective efficiency. Actually, the reduced modulus, hardness, and plasticity index decreased after the addition of POSS to coatings. This result can be ascribed to the increase of free volume of the polymer matrices upon POSS addition, as also indicated by DSC analyses. Specificaly, DSC showed a significant decrease of the glass transition temperature in the presence of POSS nanoparticles. In contrast, improvements in the abrasion resistance were noted, along with a decrease in the pile-up of matter during the applied load in nanoscratch experiments.

CRediT authorship contribution statement

Mohor Mihelčič: Investigation, Formal analysis, Data curation. **Miran Gaberšček:** Formal analysis, Software. **Martina Salzano de Luna:** Formal analysis, Data curation, Conceptualization, Writing - review & editing. **Marino Lavorgna:** Validation, Methodology, Supervision. **Chiara Giuliani:** Formal analysis, Data curation. **Gabriella Di Carlo:** Methodology, Supervision, Validation. **Angelja K. Surca:** Conceptualization, Methodology, Visualization, Writing - original draft, Writing - review & editing.

Declaration of Competing Interest

There is no financial/personal interest or belief that could affect the objectivity of this work.

Acknowledgements

This study has received funding from the European Union's Horizon 2020 research and innovation programme under grant agreement No. 646063 (NANOmaterials for the RESToration of works of ART (NANORESTART)). Dr. Cristina Riccucci and Dr. Marianna Pascucci are acknowledged for the SEM and optical analysis. Special thanks to Helena Spreizer for optical and contact angle measurements. The authors also thank Mr. Mario De Angioletti for the technical support for nanoindentation and nanoscratch analyses.

Data availability statement

All data processed herein are available on request.

Appendix A. Supplementary data

Supplementary data to this article can be found online at https://doi.org/10.1016/j.matdes.2019.107860.

References

[1] L.B. Brostoff, Coating Strategies for the Protection of Outdoor Bronze Art and Ornamentation, University of Amsterdam, 2003.

[2] T. Kosec, A. Legat, I. Milošev, The comparison of organic protective layers on bronze and copper, Prog. Org. Coat. 69 (2010) 199–206, https://doi.org/10.1016/j.porgcoat.2010.04.010.

[3] G. Masi, A. Balbo, J. Esvan, C. Monticelli, J. Avila, L. Robbiola, E. Bernardi, M.C. Bignozzi, M.C. Asensio, C. Martini, C. Chiavari, X-ray photoelectron spectroscopy as a tool to investigate silane-based coatings for the protection of outdoor bronze: the role of alloying elements, Appl. Surf. Sci. 433 (2018) 468–479, https://doi.org/10.1016/j.apsusc.2017.10.089.

[4] C. Giuliani, M. Pascucci, C. Riccucci, E. Messina, M. Salzano de Luna, M. Lavorgna, G.M. Ingo, G. Di Carlo, Chitosan-based coatings for corrosion protection of copper-based alloys: a promising more sustainable approach for cultural heritage applications, Prog. Org. Coat. 122 (2018) 138–146, https://doi.org/10.1016/j.porgcoat.2018.05.002.

[5] F. Faraldi, B. Cortese, D. Caschera, G. Di Carlo, C. Riccucci, T. de Caro, G.M. Ingo, Smart conservation methodology for the preservation of copper-based objects against the hazardous corrosion, Thin Solid Films 622 (2017) 130–135, https://doi.org/10.1016/j.tsf.2016.12.024.

[6] M. Salzano De Luna, G.G. Buonocore, C. Giuliani, E. Messina, G. Di Carlo, M. Lavorgna, L. Ambrosio, G.M. Ingo, Long-lasting efficacy of coatings for bronze artwork conservation : the key role of layered double hydroxide nanocarriers in protecting corrosion inhibitors from photodegradation, Angew. Chem. Int. Ed. 57 (2018) 7380–7384, https://doi.org/10.1002/anie.201713234.

[7] T.J. Shedlosky, A. Huovinen, D. Webster, G. Bierwagen, Development and evaluation of removable protective coatings on bronze, Proc. Met. 2004, National Museum of Australia Canberra ACT, Canberra 2004, pp. 400–413.

[8] M. Mihelčič, M. Gaberšček, G. Di Carlo, C. Giuliani, M. Salzano de Luna, M. Lavorgna, A.K. Surca, Influence of silsesquioxane addition on polyurethane-based protective coatings for bronze surfaces, Appl. Surf. Sci. 467–468 (2019) 912–925.

[9] N.A. Swartz, T. Lasseter Clare, Understanding the differences in film formation mechanisms of two comparable solvent based and water-borne coatings on bronze substrates by electrochemical impedance spectroscopy, Electrochim. Acta 62 (2012) 199–206, https://doi.org/10.1016/j.electacta.2011.12.015.

[10] G. Bierwagen, T.J. Shedlosky, K. Stanek, Developing and testing a new generation of protective coatings for outdoor bronze sculpture, Prog. Org. Coat. 48 (2003) 289–296, https://doi.org/10.1016/j.porgcoat.2003.07.004.

[11] N.A. Swartz, K.A. Wood, T. Lasseter Clare, Characterizing and improving performance properties of thin solid films produced by weatherable water-borne colloidal suspensions on bronze substrates, Prog. Org. Coat. 75 (2012) 215–223, https://doi.org/10.1016/j.porgcoat.2012.04.017.

[12] M. Mihelčič, L. Slemenik Perše, E. Šest, I. Jerman, C. Giuliani, G. Di Carlo, M. Lavorgna, A.K. Surca, Development of solvent- and water-borne fluoropolymer protective coatings for patina-free bronze discs, Prog. Org. Coat. 125 (2018) 266–278.

[13] P. Colomban, A. Tournié, M. Maucuer, P. Meynard, On-site Raman and XRF analysis of Japanese/Chinese bronze/brass patina – the search for specific Raman signatures, J. Raman Spectrosc. 43 (2012) 799–808, https://doi.org/10.1002/jrs.3095.

[14] H. Tanabe, W. Darden, M. Nagai, T. Takayanagi, The progress of newly developed fluoro-polymer topcoat systems - weathering performance and track records since the 1980 ' s, Corros. 2011, NACE International, Huston 2011, pp. NACE–11039.

[15] R. Parker, K. Blankenship, Fluoroethylene vinyl ether resins for high-performance coatings, in: K.B. Tator (Ed.), ASM Handbook, Prot. Org. Coatings, ASM International 2015, pp. 88–95.

[16] P.D. Lickiss, F. Rataboul, Fully condensed polyhedral oligosilsesquioxanes (POSS): From synthesis to application, in: A. Hill, M.J. Fink (Eds.), Adv. Organomet. Chem, Academic Press 2008, pp. 1–116, https://doi.org/10.1016/S0065-3055(08)00001-4.

[17] E. Ayandele, B. Sarkar, P. Alexandridis, Polyhedral oligomeric silsesquioxane (POSS)-containing polymer nanocomposites, Nanomaterials 2 (2012) 445–475, https://doi.org/10.3390/nano2040445.

[18] J.P. Lewicki, K. Pielichowski, M. Jancia, E. Hebda, R.L.F. Albo, R.S. Maxwell, Degradative and morphological characterization of POSS modified nanohybrid polyurethane elastomers, Polym. Degrad. Stab. 104 (2014) 50–56, https://doi.org/10.1016/j.polymdegradstab. 2014.03.025.

[19] C.J. van Oss, R.J. Good, M.K. Chaudhury, Additive and nonadditive surface tension components and the interpretation of contact angles, Langmuir 4 (1988) 884–891, https://doi.org/10.1021/la00082a018.

[20] K. Geng, F. Yang, T. Druffel, E.A. Grulke, Nanoindentation behavior of ultrathin polymeric films, Polymer (Guildf) 46 (2005) 11768–11772, https://doi.org/10.1016/j.polymer.2005.08.096.

[21] B. Du, O.K.C. Tsui, Q. Zhang, T. He, Study of elastic Modulus and yield strength of polymer thin films using atomic force microscopy, Langmuir 17 (2001) 3286–3291, https://doi.org/10.1021/la001434a.

[22] M. Rodošek, M. Koželj, L. Slemenik Perše, R. Cerc Korošec, M. Gaberšček, A.K. Surca, Protective coatings for AA 2024 based on cyclotetrasiloxane and various alkoxysilanes, Corros. Sci. 126 (2017) 55–68, https://doi.org/10.1016/j.corsci.2017.06.011.

[23] A.K. Surca, M. Rodošek, A. Kreta, M. Mihelčič, M. Gaberšček, In situ and ex situ electrochemical measurements: Spectroelectrochemistry and atomic force microscopy, in: M.H. Delville, A. Taubert (Eds.),Hybrid Org. Interfaces Towar. Adv. Funct. Mater 2018, pp. 793–838.

[24] P. Grosse, Conventional and unconventional infrared spectrometry and their quantitative interpretation, Vib. Spectrosc. 1 (1990) 187–198, https://doi.org/10.1016/0924-2031(90)80034-2.

[25] H. Ghermezcheshme, M. Mohseni, H. Yahyaei, Use of nanoindentaion and nanoscratch experiments to reveal the mechanical behavior of POSS containing polyurethane nanocomposite coatings: the role of functionality, Tribol. Int. 88 (2015) 66–75, https://doi.org/10.1016/j.triboint.2015.02.023.

[26] H. Liu, S. Zheng, Polyurethane networks nanoreinforced by polyhedral oligomeric silsesquioxane, Macromol. Rapid Commun. 26 (2005) 196–200, https://doi.org/10.1002/marc.200400465.

[27] A. Leyland, A. Matthews, Design criteria for wear-resistant nanostructured and glassy-metal coatings, Surf. Coat. Technol. 177–178 (2004) 317–324, https://doi.org/10.1016/j.surfcoat.2003.09.011.

[28] E.P. Koumoulos, C.A. Charitidis, D.P. Papageorgiou, A.G. Papathanasiou, A.G. Boudouvis, Nanomechanical and nanotribological properties of hydrophobic fl uorocarbon dielectric coating on tetraethoxysilane for electrowetting applications, Surf. Coat. Technol. 206 (2012) 3823–3831, https://doi.org/10.1016/j.surfcoat.2012.01.034.

[29] R. Consiglio, N. Randall, B. Bellaton, J. von Stebut, The nano-scratch tester (NST) as a new tool for assessing the strength of ultrathin hard coatings and the mar resistance of polymer films, Thin Solid Films 332 (1998) 151–156, https://doi.org/10.1016/S0040-6090(98)00987-0.

[30] C.A. Charitidis, Nanomechanical and nanotribological properties of carbon-based thin films : a review, Int. J. Refract. Met. Hard Mater. 28 (2010) 51–70, https://doi.org/10.1016/j.ijrmhm.2009.08.003.

[31] G. Di Carlo, C. Giuliani, C. Riccucci, M. Pascucci, E. Messina, G. Fierro, M. Lavorgna, G.M. Ingo, Artificial patina formation onto copper-based alloys: chloride and sulphate induced corrosion processes, Appl. Surf. Sci. 421 (2017) 120–127, https://doi.org/10.1016/j.apsusc.2017.01.080.

[32] G.M. Ingo, E. Angelini, T. De Caro, G. Bultrini, I. Calliari, Combined use of GDOES , SEM + EDS , XRD and OM for the microchemical study of the corrosion products on archaeological bronzes, Appl. Phys. A Mater. Sci. Process. 79 (2004) 199–203, https://doi.org/10.1007/s00339-004-2533-1.

[33] M.L. Zheludkevich, R. Serra, M.F. Montemor, I.M.M. Salvado, M.G.S. Ferreira, Corrosion protective properties of nanostructured sol – gel hybrid coatings to AA2024-T3, Surf. Coat. Technol. 200 (2006) 3084–3094, https://doi.org/10.1016/j.surfcoat.2004.09.007.

[34] M. Špirkova, J. Pavličević, A. Strachota, R. Poreba, O. Bera, L. Kapralkova, J. Baldrian, M. Šlouf, N. Lazić, J. Budinski-Simendić, Novel polycarbonate-based polyurethane elastomers: composition – property relationship, Eur. Polym. J. 47 (2011) 959–972, https://doi.org/10.1016/j.eurpolymj.2011.01.001.

[35] N. Serin, T. Serin, S. Horzum, Y. Celik, Annealing effects on the properties of copper oxide thin films prepared by chemical deposition, Semicond. Sci. Technol. 20 (2005) 398–401, https://doi.org/10.1088/0268-1242/20/5/012.

[36] M.R. Johan, M.S.M. Suan, N.L. Hawari, H.A. Ching, Annealing effects on the properties of copper oxide thin films prepared by chemical deposition, Int. J. Electrochem. Sci. 6 (2011) 6094–6104, https://doi.org/10.1088/0268-1242/20/5/012.

[37] G.W. Poling, Infrared reflection studies of metal surfaces, J. Colloid Interface Sci. 34 (1970) 365–374.

[38] L.B. Brostoff, R. de la Rie, Chemical characterization of metal/coating interfaces from model samples for outdoor bronzes by reflection-absorption infrared spectroscopy (RAIR) and attenuated total reflection spectroscopy (ATR), Proc. Int. Congr. Met. 98, James & James (Science Publishers) Ltd 1998, pp. 320–328.

[39] I. Jerman, M. Koželj, B. Orel, The effect of polyhedral oligomeric silsesquioxane dispersant and low surface energy additives on spectrally selective paint coatings with self-cleaning properties, Sol. Energy Mater. Sol. Cells 94 (2010) 232–245, https://doi.org/10.1016/j.solmat.2009.09.008.

[40] A.K. Nanda, D.A. Wicks, S.A. Madbouly, J.U. Otaigbe, Nanostructured polyurethane/POSS hybrid aqueous dispersions prepared by homogeneous solution polymerization, Macromolecules 39 (2006) 7037–7043, https://doi.org/10.1021/ma060809h.

[41] S.S. Mahapatra, S.K. Yadav, J.W. Cho, Nanostructured hyperbranched polyurethane elastomer hybrids that incorporate polyhedral oligosilsesquioxane, React. Funct. Polym. 72 (2012) 227–232, https://doi.org/10.1016/j.reactfunctpolym.2012.02.001.